Hydrogen dissociation on metal surfaces

Wijzenbroek, M.

CHAPTER 3

Static surface temperature effects on the dissociation of H_2 and D_2 on Cu(111)

This chapter is based on:

M. Wijzenbroek and M. F. Somers. Static surface temperature effects on the dissociation of H_2 and D_2 on Cu(111). *Journal of Chemical Physics* **137**(5), 054703, 2012.

3.1 Introduction 52
3.2 Static corrugation model 55
Model overview 56 • Method 57 • Computational details 62
3.3 Results and discussion 63
1D correction function 64 • Initial state-resolved reaction probability 66 • Rotational quadrupole alignment parameter 81 • Molecular beams 84
3.4 Conclusions 86
References 88

Abstract

A model for taking into account surface temperature effects in molecule–surface reactions is reported and applied to the dissociation of H_2 and D_2 on Cu(111). In contrast to many models developed before, the model constructed here takes into account the effects of static corrugation of the PES rather than energy exchange between the impinging hydrogen molecule and the surface. Such an approximation is a vibrational sudden approximation. The quality of the model is assessed by comparison to a recent DFT study. It is shown that the model gives a reasonable agreement with recently performed *ab initio* molecular dynamics calculations, in which the surface atoms were allowed to move. The observed broadening of the reaction probability curve with increasing surface temperature is attributed to the displacement of surface atoms, whereas the effect of thermal expansion is found to be primarily a shift of the curve to lower energies. It is also found that the rotational quadrupole alignment parameter is generally decreased at low energies, whereas it remains approximately constant at high energies. Finally it is shown that the approximation of an ideal static surface works well for low surface temperatures, in particular for the molecular beams for this system ($T_s = 120\,\mathrm{K}$). Nonetheless, for the state-resolved reaction probability at this surface temperature, some broadening is found.

3.1 Introduction

One of the most studied systems in surface chemistry is the dissociation of hydrogen on a copper surface. In this work the Cu(111) face is considered; a large number of theoretical[1–21] and experimental[22–34] studies have been done for this particular surface. Theoretical studies have mostly considered motion only in the degrees of freedom of the hydrogen molecule, due to the complexity of taking into account surface degrees of freedom. In experiments, however, often high surface temperatures are applied. Instead of treating the full system, in most previous theoretical work the atoms in the surface have been assumed to be fixed to their ideal lattice positions. This approximation is expected to hold as long as the surface temperature is relatively low, but may be suspect at

high temperatures for specific observables because significant surface temperature effects were found in experiments.[27,30]

Calculations with the Born–Oppenheimer static surface (BOSS) model have provided a very good description of the experiments.[1,2] A number of approximations are made within this model. First, the surface atoms are frozen at their ideal lattice positions. Second, electron–hole pair excitations are neglected. Finally, density functional theory (DFT) is used to compute the potential energy surface (PES). Electron–hole pair excitations should not be important for hydrogen dissociating on a metal surface.[35] Recently an accurate specific reaction parameter (SRP) DFT functional was found for this system by taking a linear combination of two functionals often used for the description of molecule–surface reactions.[1,2] In this study, a number of the remaining discrepancies between theory and experiment were attributed to the neglect of phonons. For example, the rotational quadrupole alignment parameter can be expected to be dependent on the surface temperature, because a corrugated surface may allow tilted molecules that do not react on an ideal surface to react due to the surface being locally tilted. The dependence of the rotational quadrupole alignment parameter on the surface temperature has however not been measured experimentally.

The remaining discrepancies between theory and experiment therefore make it interesting to take into account the surface degrees of freedom. Although it is now possible to take into account surface temperature effects with *ab initio* molecular dynamics (AIMD),[20,21,36] these calculations are still computationally expensive, restricting the scope of these studies. It is therefore desirable to have a model which is computationally less expensive. Additionally, using a model allows a more thorough assignment of observed effects in the dynamics to structural changes caused by the surface temperature, as individual parts of a model can be switched off more easily.

In order to construct such a model efficiently, it is important to first consider precisely how surface temperature influences the atomic structure of the system. One of the most well known effects is thermal expansion, *i.e.*, the crystal expands as the surface temperature is increased.[37,38] Additionally, at the surface the interlayer spacings may be different from interlayer spacings in the bulk, and they may be temper-

ature dependent.[39] These two effects combined can be referred to as systematic (static) effects, as they involve systematic displacements of atoms in the crystal. The surface atoms will additionally vibrate around their ideal lattice positions, giving the surface atoms an instantaneous displacement.[40,41] This is a statistical effect, due to the (apparent) random displacement of atoms in the crystal. Additionally there will be dynamical effects involving the motion of surface atoms, such as energy exchange between the impinging hydrogen molecule and the surface and dissipation of heat through the crystal.

Work on surface temperature effects has mostly focused on energy exchange with surface oscillator (SO)[42–48] models, of which the most advanced study so far for hydrogen dissociating on Cu(111) has been the application[1,2] of a three-dimensional (3D) SO model.[48] It was however found that this does not account sufficiently for the effects observed experimentally.[1,2] Attempts have been made to improve the SO model. The modified surface oscillator (MSO)[42,44] model contains a microscopically motivated coupling term. Nave and Jackson[49,50] recently showed that the harmonic approximation used in the SO model is reasonable. Another model which has been applied is the surface mass (SM)[46,47] model, in which the surface does not oscillate but instead is given a certain velocity and mass, which does not allow energy exchange, but does allow recoil effects to be taken into account. Also, for H_2 dissociation on Pd(111), an extension of the corrugation reducing procedure (CRP) has been applied.[51] Finally, Bonfanti *et al.*[52] performed seven-dimensional (7D) quantum dynamics (QD) calculations for H_2 dissociation on Cu(111), in which a second layer atom was allowed to move perpendicular to the surface. In this study, calculations were additionally performed using a vibrational sudden approximation (6+1D), and reaction probabilities computed using this model were found to be in good agreement with the full 7D results.

In this chapter a model is developed to take into account the thermal displacement of surface atoms and the expansion of the crystal within a vibrational sudden approximation, in which the surface atoms are assumed to be fixed but not in their ideal positions. The model is then tested by comparison with a DFT study[53] for this system in which the influence of surface atom displacements is considered. Additionally,

three observables are computed and the results are compared, where possible, to experiments. The initial state-resolved reaction probability is considered, because for this observable strong surface temperature effects are known from experiments. These effects are manifested in the broadening of the reaction probability curves with increasing surface temperature.[27,30] Also the rotational quadrupole alignment parameter is considered, because surface temperature effects are expected for this observable. Finally, to verify the approximation previously made of an ideal static crystal being representative of a crystal at low temperatures, molecular beams are simulated to compute sticking probabilities.

The structure of this chapter is as follows. In section 3.2.1 an overview and motivation of the model that was constructed is provided, and the individual parts of the model are discussed in section 3.2.2. In section 3.2.3 the computational details of the calculations that were performed are given. Then in section 3.3 the results that were obtained by application of the model are discussed. This section is split in several parts for the different observables that are considered in the present work. First, in section 3.3.1, the quality of the model is assessed by comparison to the DFT study[53] mentioned above. In section 3.3.2 the initial state-resolved reaction probability is considered, then in section 3.3.3 the rotational quadrupole alignment parameter, and finally sticking probabilities are discussed in section 3.3.4. In section 3.4 the conclusions are given.

3.2 Static corrugation model

In this section the newly developed static corrugation model is described and arguments are made to support the assumptions made in the construction of the model. First a general overview of the model is given, after which a more detailed description is given. Finally the computational details and scope of the present study, the application to H_2 dissociation on Cu(111), are given.

3.2.1 Model overview

Previous work on the surface temperature effects of H_2 dissociation on Cu(111) has focused on the effects of energy exchange through SO models.[42–48] In SO models the entire surface is attached to a spring. As the impinging hydrogen molecule approaches the surface it can interact with the surface by exchanging energy with the oscillating surface. It has been shown that a SO model alone cannot quantitatively describe the broadening of the sticking curves as observed in experiment.[1,2]

In previous other work, mostly ideal static lattices were considered and these were assumed to be representative of a real crystal at 0 K. Results based on this model were compared with experiments done at higher temperatures ($120 - 925$ K). Such a treatment of an ideal lattice is however somewhat misleading as the surface atoms in a real 0 K crystal will not necessarily be in their ideal positions,[40,41] due to the presence of zero-point energy (ZPE) in the surface. In order to model a real 0 K crystal, the static surface approximation has to be dropped, so that the surface atoms can move due to their ZPE and energy exchange between the hydrogen molecule and the copper surface can take place. At a higher temperature, the atoms will vibrate even more and, additionally, thermal expansion may have to be taken into account.

A number of approximations are argued here to be reasonable. First of all, due to the large mass mismatch between the hydrogen molecule and the surface atoms, motion of the hydrogen molecule and the surface atoms should only be weakly coupled, *e.g.*, the effect of energy exchange should be small. Second, surface atoms move relatively slowly compared to the hydrogen molecule. This indicates that a sudden approximation, in which the surface atoms are assumed fixed but not in their ideal positions, should work well. Finally, in typical experiments the time between scattering events is long compared to a scattering event. The time between scattering events is long, as shown by the adsorption and desorption rates, which are on the order of monolayers per second.[29,32] This indicates that there is no clear correlation between the surfaces different hydrogen molecules "see".

Further motivation for these approximations can be derived from recent studies of CH_4 dissociation on Ni and Pt surfaces.[49,50,54,55] It was

found that only very little energy exchange occurs (20 meV at an incidence energy of 1 eV at a surface temperature of 475 K for dissociation on Ni(111)), even though CH_4 is significantly closer in mass to Ni than H_2 is to Cu ($m_{Ni}/m_{CH_4} = 3.7$, $m_{Cu}/m_{H_2} = 31.5$).

For the system considered here, hydrogen dissociation on Cu(111), a model is therefore constructed for a non-ideal but still fixed surface, in which different surface configurations are taken into account for different scattering events. It is noted that the model discussed in this chapter can in principle be combined with the SM model[46,47] so that also recoil effects can be taken into account.

3.2.2 Method

3.2.2.1 Potential energy surface

The PES for a diatomic molecule in the vicinity of a surface can be written as[53]

$$V(\vec{r},\vec{q}) = V^{6D}(\vec{r};\vec{q}_{id}) + V_{coup}(\vec{r},\vec{q}) + V_{strain}(\vec{q}), \tag{3.1}$$

in which V^{6D} is the 6D PES of the diatomic molecule in the presence of an ideal surface, V_{coup} the so-called coupling potential, which is defined by this equation, and V_{strain} the strain in the surface defined by $V_{strain}(\vec{q}) = V_{slab}(\vec{q}) - V_{slab}(\vec{q}_{id})$. Here, V_{slab} is the potential energy of the slab in absence of the diatomic molecule (or with the diatomic molecule far away from the surface). The coordinates $\vec{r}$ are those of the diatomic molecule, and $\vec{q}$ are the coordinates of all surface atoms, with $\vec{q}_{id}$ the coordinates of the surface atoms in their ideal lattice positions. The representation of the 6D potential is now well understood; a variety of methods, such as the CRP,[56] have been developed for representing or interpolating this part of the potential. The coupling potential contains by far the most information, relating the $\vec{r}$ and $\vec{q}$ degrees of freedom. Bonfanti *et al.*[53] computed the coupling potential for H_2 dissociation on Cu(111) using DFT for a number of configurations, in which the H_2 molecule was fixed at barrier locations above the high symmetry sites while a single surface atom was moved in a particular direction. It was noted in this study that the dependence of the coupling poten-

tial on different surface degrees of freedom is, to within a reasonable approximation, additive.

From equation (3.1) a correction term can be determined for displacement of surface atoms:

$$\begin{aligned} V_{\text{corr}}(\vec{r},\vec{q}) &= V(\vec{r},\vec{q}) - V(\vec{r},\vec{q}_{\text{id}}) \\ &= V_{\text{int}}(\vec{r},\vec{q}) - V_{\text{int}}(\vec{r},\vec{q}_{\text{id}}) + V_{\text{strain}}(\vec{q}), \end{aligned} \tag{3.2}$$

as $V_{\text{coup}}(\vec{r},\vec{q}_{\text{id}}) = 0$, $V_{\text{strain}}(\vec{q}_{\text{id}}) = 0$ and $V^{6\text{D}}$ does not depend on surface degrees of freedom. Here the substitution

$$V_{\text{coup}}(\vec{r},\vec{q}) = V_{\text{int}}(\vec{r},\vec{q}) - V_{\text{int}}(\vec{r},\vec{q}_{\text{id}}) \tag{3.3}$$

has been made, in which V_{int} is a term describing the interaction between the hydrogen molecule and the copper atoms. The correction term has to be added to $V^{6\text{D}}$. For static slab simulations V_{strain} does not have to be taken into account in equation (3.2). It is however needed to get V_{coup} in equation (3.2) and thus implicitly V_{int} through equation (3.3).

Due to the large number of degrees of freedom, it is difficult to treat any of the correction terms $V_{\text{int}}(\vec{r},\vec{q})$ exactly. It may, however, be possible to use some kind of approximate analytical form. A logical choice for this form would be a small number of terms from the many-body expansion[57] of the full PES of equation (3.1).

Consider a general PES $E_M(\vec{R}_1,\vec{R}_2,\ldots,\vec{R}_M)$ for a system of M atoms. In the many-body expansion this PES is written as a sum of N-body potential terms with N up to the number of atoms considered in the full PES:[57]

$$E_M(\vec{R}_1,\vec{R}_2,\ldots,\vec{R}_M) = \sum_{N=0}^{M} E^{(N)}(\vec{R}_1,\vec{R}_2,\ldots,\vec{R}_M), \tag{3.4}$$

and each individual energy term, $E^{(N)}$, can be written as

$$E^{(N)}(\vec{R}_1,\vec{R}_2,\ldots,\vec{R}_M) = \frac{1}{N!}\sum_{m_1}^{M}\sum_{m_2}^{M}\ldots\sum_{m_N}^{M} V^{(N)}(\vec{R}_{m_1},\vec{R}_{m_2},\ldots,\vec{R}_{m_N}). \tag{3.5}$$

This expression is exact and does not provide a simplification. One could however expect that the lowest order terms are the most important ones. Expressions like this are commonly used in force fields and recently reactive force fields have been applied to molecule–surface reactions with reasonable success, as long as the force field is specifically parametrized for the description of a molecule–surface reaction.[58–61] Applying the many-body expansion to an H_2 molecule near a Cu surface with n surface atoms, if only two-body terms are included in the expansion the full potential can be written as

$$V(\vec{r},\vec{q}) = V^{(2)}_{\mathrm{H-H}}\left(\left|\vec{R}_{\mathrm{H_1}} - \vec{R}_{\mathrm{H_2}}\right|\right) + \sum_{I}^{2}\sum_{i}^{n} V^{(2)}_{\mathrm{H-Cu}}\left(\left|\vec{R}_{\mathrm{H_I}} - \vec{R}_{\mathrm{Cu_i}}\right|\right) + \sum_{i}^{n}\sum_{j>i}^{n} V^{(2)}_{\mathrm{Cu-Cu}}\left(\left|\vec{R}_{\mathrm{Cu_i}} - \vec{R}_{\mathrm{Cu_j}}\right|\right), \tag{3.6}$$

in which $V^{(2)}_{\mathrm{H-H}}$ is the interaction between the two hydrogen atoms, $V^{(2)}_{\mathrm{H-Cu}}$ the interaction between a hydrogen atom and a copper atom, and $V^{(2)}_{\mathrm{Cu-Cu}}$ the interaction between two copper atoms. Therefore, within the two-body approximation, using equation (3.6) in equations (3.2) and (3.3),

$$V_{\mathrm{int}}(\vec{r},\vec{q}) = \sum_{I}^{2}\sum_{i}^{n} V^{(2)}_{\mathrm{H-Cu}}\left(\left|\vec{r}_I - \vec{q}_i\right|\right), \tag{3.7}$$

$$V_{\mathrm{slab}}(\vec{q}) = \sum_{i}^{n}\sum_{j>i}^{n} V^{(2)}_{\mathrm{Cu-Cu}}\left(\left|\vec{q}_i - \vec{q}_j\right|\right). \tag{3.8}$$

It is again emphasized that this last term V_{slab} is not needed for a static surface simulation.

3.2.2.2 Fitting procedure

The form chosen for $V^{(2)}_{\mathrm{H-Cu}}$ is

$$V^{(2)}_{\mathrm{H-Cu}}(r) = (1-\rho(r))V(r) + \rho(r)V(b_2), \tag{3.9}$$

where

$$V(r) = -e^{-l(r-z)} \cdot \sum_{k=0}^{3} \left(c_k (r-z)^k\right) \tag{3.10}$$

and

$$\rho(x) = \begin{cases} 0 & \text{if } x < b_1 \\ \frac{1}{2}\cos\left(\frac{\pi(x-b_2)}{b_2-b_1}\right) + \frac{1}{2} & \text{if } b_1 \leq x \leq b_2 \\ 1 & \text{if } x > b_2. \end{cases} \tag{3.11}$$

The form of the 1D potential $V^{(2)}_{\mathrm{H-Cu}}(r)$ is therefore Rydberg-like with an added switch function. Correct parameters for equations (3.10) and (3.11) were found by fitting $V_{\mathrm{coup}}(\vec{r}, \vec{q})$ (equation (3.3)) directly to DFT data of Bonfanti *et al.*[53] The resulting fit is discussed in section 3.3.1.

3.2.2.3 Surface configurations

As the strain term in equation (3.2) is at present not included, the surface atoms cannot move and surface configurations cannot be generated trivially. Therefore an alternative method is used, based on the Debye–Waller (DW) B factor. To randomly displace surface atoms, surface atom position vectors are defined by

$$\vec{q}_i = \vec{q}_{\mathrm{id},i} + q_i \hat{u}_i, \tag{3.12}$$

where $\vec{q}_{\mathrm{id},i}$ is the surface atom position vector for an ideal surface associated with atom i, $\hat{u}_i$ is a 3D unit vector with a random orientation and q_i a randomly chosen scalar displacement sampled from a Gaussian distribution with width

$$\sigma = \sqrt{\frac{3B}{8\pi^2}}. \tag{3.13}$$

In this formula B is the DW factor for a particular surface temperature. The used DW factors are obtained from fits[40] to experimental neutron inelastic scattering data.[41] The approximations made here are that the displacement is assumed to be isotropic and bulk-like, so any surface

effects are neglected. Displacements obtained from the DW factor are in agreement with displacements obtained from harmonic fits to the strain potential;[53] with the DW factor $\sigma = 0.2547$ Å at $T_s = 925$ K, while for the harmonic fits $\sigma = 0.25$ Å for first layer perpendicular motion ($\omega = 16$ meV) and $\sigma = 0.21$ Å for second layer perpendicular motion ($\omega = 19$ meV) at the same surface temperature.

Only surface atoms within a radius of $16\,a_0$ of the projection of the center of mass of the initial configuration of the H_2 molecule on the surface are displaced from their ideal positions using this method. In table 3.1 the parameter σ is shown for the surface temperatures that are considered.

3.2.2.4 Thermal expansion and contraction/expansion of the first layer

Taking into account systematic displacements like thermal expansion is less straightforward. If a correction is made by adjusting the displaced surface atom position vectors using equation (3.2), the proper symmetry of the system is not kept. This is because the surface also expands in the surface plane and the two-body approximation is not exact, which means that the potential energy not accounted for by the two-body approximation on sites which should be equal could be different.

A possible way of taking thermal expansion into account is by removing the part of the potential energy that can be accounted for by the two-body approximation from the full V^{6D}, "stretching" the residual function in X and Y by the same factor as the expansion that occurs, and finally re-adding the part that can be accounted for by the two-body approximation:

$$V(\vec{r}_{exp}, \vec{q}_{exp}) = V^{6D}(\vec{r'}; \vec{q}_{id}) - V_{int}(\vec{r'}, \vec{q}_{id}) + V_{int}(\vec{r}_{exp}, \vec{q}_{exp}). \qquad (3.14)$$

It is pointed out here that $\vec{r'}$ and $\vec{r}_{exp}$ depend on each other. $\vec{r'}$ is related to $\vec{r}_{exp}$ so that $X' = X_{exp}/\alpha$ and $Y' = Y_{exp}/\alpha$. Here α is L_{exp}/L_{id}. Z', r', ϑ' and φ' are equal to Z_{exp}, r_{exp}, ϑ_{exp} and φ_{exp}.

As there is no periodicity perpendicular to the surface, changing interlayer distances can simply be done by changing $\vec{q}$. To correct for

Table 3.1 Model parameters σ, α and d_{1-2} as used for the surface temperatures considered in this work. These parameters were derived from experimental results.[37–41]

T_s (K)	σ (Å)	α	d_{1-2} (Å)
0	0.0746	1.0000	2.1200
120	0.0993	1.0001	2.1212
300	0.1470	1.0034	2.1270
600	0.2056	1.0087	2.1297
925	0.2547	1.0152	2.1739

Table 3.2 Rovibrational states for which calculations have been performed. In the molecular beam simulations of section 3.3.4, all these states are included in the calculations.

Vibration	Rotation D_2	Rotation H_2
$v = 0$	$J = 0 \ldots 15$	$J = 0 \ldots 11$
$v = 1$	$J = 0 \ldots 12$	$J = 0 \ldots 7$
$v = 2$	$J = 0 \ldots 10$	No calculations

changes in the first interlayer spacing, all atoms below the first layer were translated up or down so that the first interlayer distance has a particular value d_{1-2}. Because in the present model the 1D interaction $V^{(2)}_{H-Cu}$ is switched off beyond about $7.5\,a_0$, effectively only the change in interlayer distance between the first two layers can be taken into account. In table 3.1 the parameters α and d_{1-2} are shown for the surface temperatures that are considered. These parameters were computed based on experimental data.[37–39]

3.2.3 Computational details

The reaction probability was sampled for each initial rovibrational state at 20 incidence energies, spread equidistantly from 0 eV up to 1 eV. Only normal incidence is considered. The considered surface temperatures are 0 K, 120 K, 300 K, 600 K and 925 K. Additionally, calculations were also performed for an ideal lattice. Calculations were performed both with and without the model for thermal expansion. For each incidence

energy, rovibrational state and surface temperature at least 2×10^4 trajectories were computed, spread equally over the different m_J states. Rovibrational states for which calculations have been performed are listed in table 3.2.

The SRP PES used by Díaz *et al.*[1,2] was used. This PES is a linear combination of two PESs interpolated with the CRP,[56] one based on calculations with the PW91 exchange–correlation (XC) functional,[62] the other based on calculations with the RPBE XC functional.[63] This PES has p6mm symmetry rather than p3m1 symmetry.[64]

The applied quasi-classical trajectory (QCT) method is mostly the same as used in a previous study.[1,2] The initial rovibrational energies of the H_2 molecule were computed with the Fourier grid Hamiltonian method.[65] The Hamilton equations of motion were solved by using the extrapolation method of Stoer and Bulirsch.[66] The initial angular momentum of the H_2 molecule is fixed by $L = \sqrt{J(J+1)}\hbar$. For $J > 0$, the orientation is chosen randomly by $\cos\vartheta_L = m_J/\sqrt{J(J+1)}$, where ϑ_L is the angle between L and the axis perpendicular to the surface. The center of mass of the hydrogen molecule was initially placed 9 Å away from the surface. Reaction is considered to have occurred when the H–H distance r is larger than 2.25 Å. Scattering is considered to have occurred when the hydrogen molecule has a momentum away from the surface and is further than 9 Å away from the surface. Trajectories were stopped after 20 ps. Trajectories that have not shown reaction or scattering after this time are also considered non-reactive. This choice has been made because of the static surface approximation. Although the molecule can be considered to be "trapped" in this case, motion of the surface likely leads to desorption of the trapped molecule in most cases.

3.3 Results and discussion

In this section, first the quality of the model is assessed by comparison to a recent DFT study.[53] After this assessment, a comparison is made between calculations performed on an ideal static surface, calculations performed on a non-ideal static surface with the static corrugation model (section 3.2; both with and without thermal expansion), recent AIMD results[20] and experiments. To do this, three observables are

considered: the initial state- and energy-resolved reaction probability; the energy resolved rotational quadrupole alignment parameter; and the reaction probability averaged over the velocity distribution and the rovibrational states present in molecular beams.

3.3.1 1D correction function

The 1D correction function ($V^{(2)}_{\mathrm{H-Cu}}(r)$ in equation (3.9)) used in the model is related to the coupling potential as shown in equation (3.3). As the 1D correction function to be used is fitted to reproduce the coupling potential, comparing the coupling potential computed with DFT with the coupling potential computed with the model provides a way to check the quality of the fit. In total 153 points of the coupling potential were used in the fit. Some of these points are published[53] while others are not.[67] 43 points are related to perpendicular motion of the first layer atom, 50 to perpendicular motion of the second layer atom, 44 to perpendicular motion of the third layer atom and 16 to parallel motion of the first layer atom.

In figure 3.1 the coupling potential as predicted by the model is compared with the coupling potential computed by Bonfanti *et al.*[53,67] For the first and second layer perpendicular motion the agreement is quite good, in particular for small displacements, with perhaps the exception of second layer perpendicular motion with the hydrogen molecule fixed on the TtB site. For the parallel configurations[67] the agreement is less good. The reason for this is not clear. It could be that these data points sample a different regime of r which cannot be well represented due to restrictions of the form chosen for the 1D correction function. It is noted here that only a small number of points corresponding to parallel displacement (16) are included in the fit, and as such not enough weight may be put on parallel displacement in the fit. The model can clearly not reproduce parallel motion A, and for parallel motions B, C and H the agreement is also not so good. For parallel motions D to G however, the agreement between the model and the DFT calculations is quite good. Bonfanti *et al.*[53] argued that perpendicular motion of second layer atoms has the most effect on the lowest barrier for reaction.

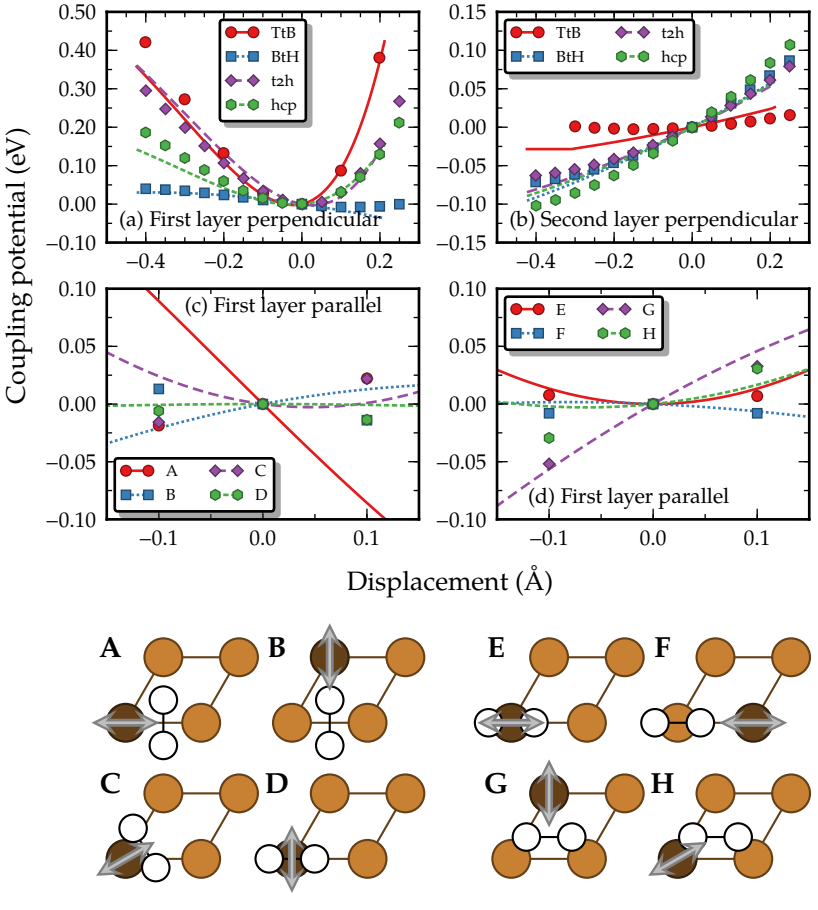

Figure 3.1 Coupling potential computed with the model (lines) compared with the coupling potential computed by Bonfanti *et al.*[53] (points) for a number of motions. For the perpendicular displacement, the hydrogen molecule is fixed at a barrier position as indicated in the graph, while a surface atom is moved in a perpendicular direction. Data for the third layer motion is not plotted as it is zero due to the added switch function. The bottom graphs represent unpublished data[67] for 8 configurations in which a first layer atom is moved in a parallel direction. These configurations are described in the bottom figure.

Table 3.3 Parameters used for the 1D correction function as defined in equations (3.9) to (3.11).

Parameter	Value
z	$2.301\,a_0$
l	$1.274/a_0$
c_0	$-0.030\,30\,E_\mathrm{h}$
c_1	$0.1035\,E_\mathrm{h}/a_0$
c_2	$-0.069\,25\,E_\mathrm{h}/{a_0}^2$
c_3	$-4.135\times10^{-9}\,E_\mathrm{h}/{a_0}^3$
b_1	$7.444\,a_0$
b_2	$7.464\,a_0$

The conclusion is therefore that a pair potential can represent quite well the behaviour of the coupling potential for perpendicular motion, and that for parallel motion the agreement is perhaps less good, but it is possible that the agreement can be improved if more configurations are added into the fit. It is even possible to extend the model to include three-body terms in V_int although this does increase the computational cost of using such a model. The agreement could also be improved by using a layer-dependent 1D correction function. This would allow a better description of the various ranges of r spanned by different motions and might also improve the agreement for first layer parallel motion. Both of these extensions require more DFT points than are used at present.

The fitted parameters are given in table 3.3. The function is also plotted in figure 3.2. It should be clear the interaction is relatively long range, up to approximately $7.5\,a_0$, which suggests it is important to take into account many surface atoms in equation (3.2).

3.3.2 Initial state-resolved reaction probability

Experimentally, Michelsen *et al.*,[28,29] Murphy and Hodgson,[30] and Rettner *et al.*[32] have measured desorption probabilities for H_2 and D_2 desorbing into a specific rovibrational state and, by invoking detailed balance, fitted the corresponding reaction probabilities to expressions

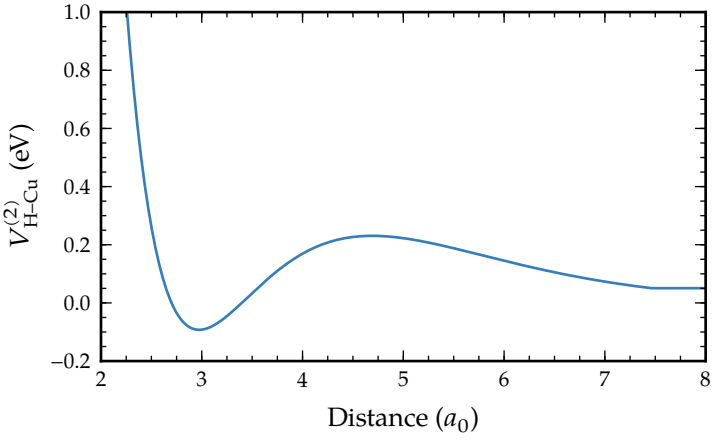

Figure 3.2 The 1D correction function $V^{(2)}_{\mathrm{H-Cu}}(r)$ based on the parameters of table 3.3.

of the form

$$R(E_{\mathrm{trans}};\nu,J) = \frac{A(\nu,J)}{2}\left(1+\mathrm{erf}\left(\frac{E_{\mathrm{trans}}-E_0(\nu,J)}{W(\nu,J)}\right)\right), \qquad (3.15)$$

in which E_{trans} is the translational energy of the H_2 molecule, $A(\nu,J)$ the saturation value of the reaction probability, $E_0(\nu,J)$ the translational energy for which the reaction probability is half the saturation value (the "dynamical barrier height") and $W(\nu,J)$ a width parameter that describes the steepness of the curve. The experimentalists found E_0 to be approximately independent of T_s, while they found W to increase with increasing T_s.

Reaction probabilities for adsorption from an initial state were computed for all states and surface temperatures listed in section 3.2.3 and these are compared to the available experimental data.

3.3.2.1 Thermal displacement

In figure 3.3 the reaction probability for a number of initial rovibrational states is shown, with only thermal displacement taken into account. If the surface temperature is increased, at low energies the reaction prob-

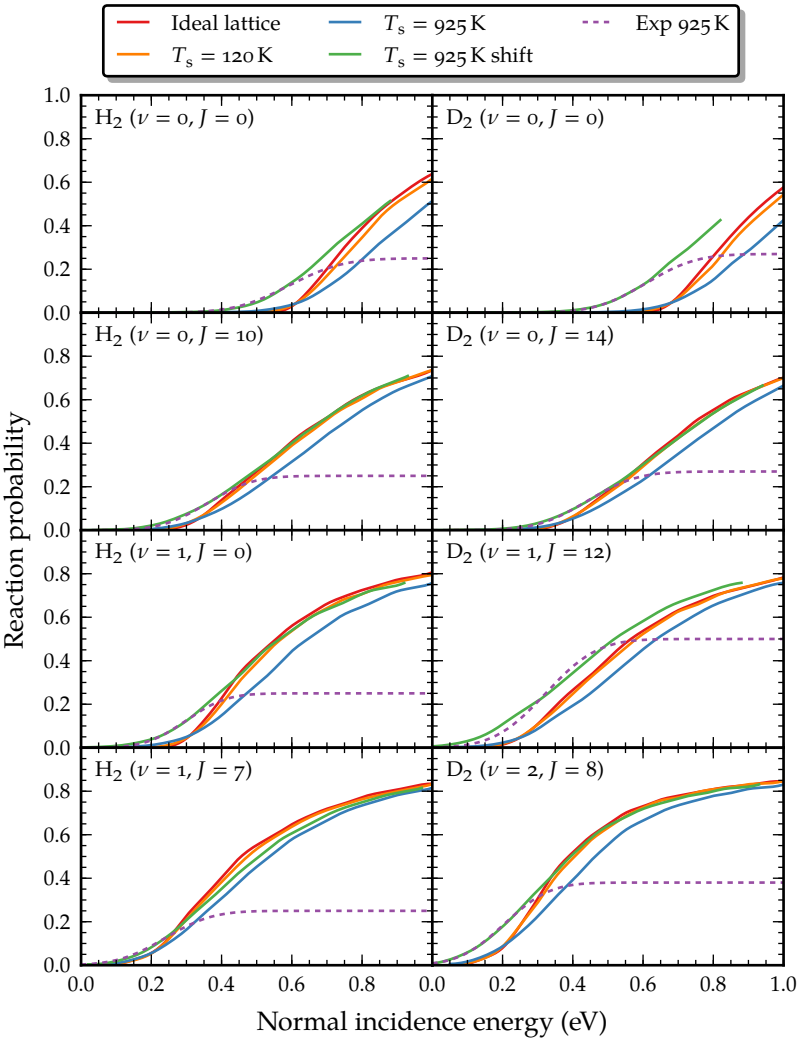

Figure 3.3 Broadening of the sticking curves as the surface temperature is increased, for a selection of initial rovibrational states, only taking into account the effects of thermal displacement. Also plotted are the experimental sticking curves obtained by Michelsen *et al.*[28,29] and Rettner *et al.*[32]

ability in general is slightly increased, whereas at high energies the reaction probability is decreased. In other words, a broadening occurs. As argued in a previous study,[1,2] there should not be a large difference between the ideal lattice and a real crystal at a low temperature. The findings here are consistent with that, although some broadening is observed for $T_s = 120\,\mathrm{K}$. The available experimental data[28,29,32] was obtained for a surface temperature $T_s = 925\,\mathrm{K}$. The agreement with the experiments generally is improved for the width (shape) of the curve, but not for the dynamical barrier height (E_0). Generally the curve is shifted too much to higher energies, *i.e.*, the system is found to not be reactive enough. To compare the width and shape of the computed $T_s = 925\,\mathrm{K}$ reaction probability curves with the experimentally measured sticking curves, the computed $T_s = 925\,\mathrm{K}$ reaction probability curves are also plotted shifted to lower energies in such a way that agreement is obtained at the experimental E_0. The agreement for the shape at low energies is excellent, except for ($\nu = 1$, $J = 12$) D_2, where the computed reaction probability curve seems to be slightly too broad.

The trends found in figure 3.3 are general for all initial states and surface temperatures considered. To emphasize this point, in figure 3.4 the reaction probability of D_2 initially in the ($\nu = 0$, $J = 11$) and ($\nu = 1$, $J = 6$) states for all surface temperatures considered is shown. As the surface temperature is increased, the sticking curve gradually broadens, increasing the reaction probability at low incidence energies, while decreasing the reaction probability at high incidence energies. All curves seem to intersect at one point close to the experimental E_0 value, and at this point the reaction probability for ($\nu = 0$, $J = 11$) is approximately 0.04 and for ($\nu = 1$, $J = 6$) is approximately 0.1. This finding is qualitatively consistent with the experiments, where it is known that the E_0 parameter of the sticking curve does not depend significantly on the surface temperature.[30,32] The experimentally obtained reaction probability for the intersection point is, however, higher. The calculations also indicate that the reaction probability does not saturate, in contrast to what is found in experiments. This discrepancy could possibly be explained by the low population of hydrogen molecules desorbing from the surface with high energies. As equation (3.15) has a saturation inherent to the form, and there is only a small weight attached to the high energy

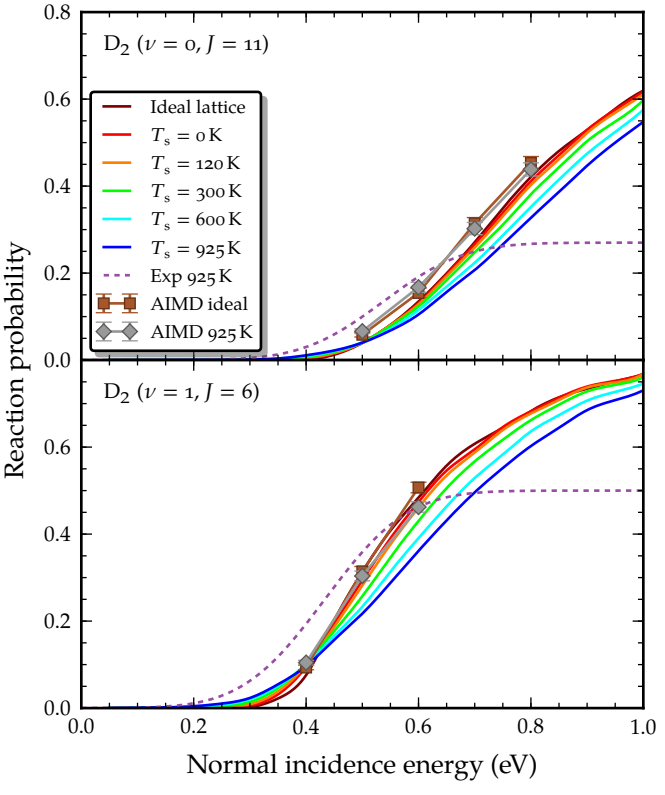

Figure 3.4 Broadening of the sticking curve for D_2 initially in the ($\nu = 0$, $J = 11$) and ($\nu = 1$, $J = 6$) states, for all considered surface temperatures, only taking into account the effects of thermal displacement. The experimental sticking curve[29] is also plotted, as well as the AIMD results by Nattino *et al.*[20]

data, the predicted fit parameters could be wrong.

The trends found for ($\nu = 0$, $J = 11$) and ($\nu = 1$, $J = 6$) D_2 are also generally valid for all states. The intersection point is found to be at a reaction probability of approximately 0.04 to 0.1 for D_2, while for H_2 it is found at reaction probabilities of up to 0.15. It seems clear that the displacement of surface atoms alone does not yield a good enough description of the process, although it does seem to account for (most of) the broadening. This can be understood as follows. Displacement of surface atoms will modulate the barrier height and position.[53] Therefore,

under the influence of thermal displacement, for each configuration of the surface atoms, some barrier heights will be decreased, while others will be increased. At low incidence energies, when only very few molecules react, an increase of the barrier will not change the results considerably, however a decrease of the barrier will make more trajectories reactive. At higher energies, when almost all molecules react, a decrease of the barrier will not change the results considerably, but an increase of the barrier will make fewer trajectories reactive. The net effect of averaging over surface configurations is therefore an increase of reactivity at low incidence energies and a decrease of reactivity at high incidence energies, in other words, a broadening. The amount of broadening is determined by the magnitude of the change in barrier height, while the point with respect to which broadening occurs (the intersection point) is determined by the precise distribution of barriers for all possible surface configurations.

The effects found for ($\nu = 0, J = 11$) and ($\nu = 1, J = 6$) D_2 are larger than those found in the AIMD study by Nattino *et al.*[20] The reaction probability curves found in the present study seem to be broader than those found by AIMD. The reason for this is not fully clear. As argued in section 3.2.1, due to the relatively slow desorption speed from the metal surface, there is a long time between different scattering events, and different hydrogen molecules therefore meet surface configurations which are not clearly related to each other. Nattino *et al.*[20] used snapshots from 1 ps dynamics simulations of eight different slabs as initial configuration of the surface, from which one is selected at random. In this study, a new surface configuration is generated for every trajectory from a distribution based on experiments. It is possible that snapshots from a 1 ps dynamics simulation are not different enough from each other, or that not enough slabs have been used, but this is not fully clear. Additionally, in the AIMD calculation a unit cell of finite size is used and periodic boundary conditions are applied while this is not assumed in the calculations on the static corrugation model. The size of the unit cell could be important due to the relatively long range interaction of $V^{(2)}_{\mathrm{H-Cu}}(r)$ (see figure 3.2).

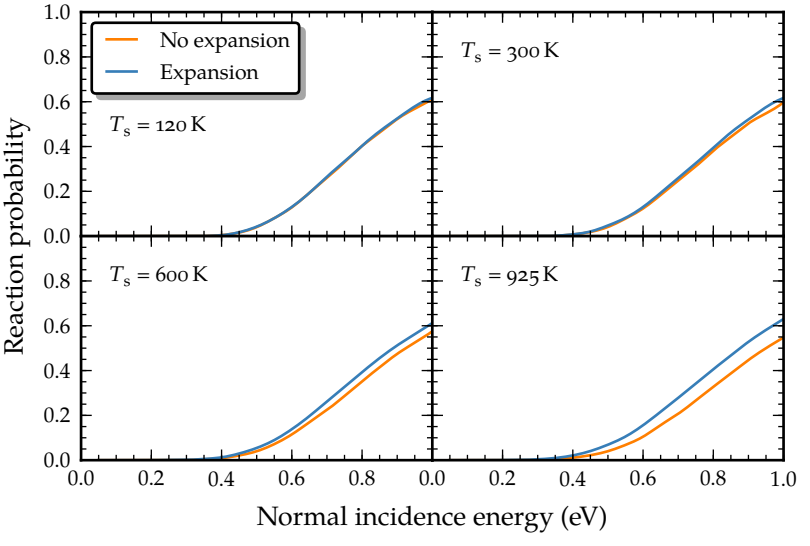

Figure 3.5 Thermal expansion effects for all surface temperatures considered for D_2 initially in the ($\nu = 0, J = 11$) state.

3.3.2.2 Thermal expansion and change in first interlayer distance

In figure 3.5 an overview is provided for thermal expansion effects for D_2 initially in the ($\nu = 0, J = 11$) state for all four surface temperatures that are considered. The results show that the most important effect is a shift of the reaction probability curve to lower energies. The size of this shift increases as the surface temperature is increased, being almost non-existent at $T_s = 120\,\mathrm{K}$, but significant at $T_s = 925\,\mathrm{K}$. Additionally, the shape of the curve is also somewhat altered: the curve is slightly narrower when thermal expansion effects are taken into account. This can be explained as follows. As the effect of the inclusion of non-ideal surface configurations is an increase of the corrugation of the PES, causing the broadening of the reaction probability curve, expansion of the crystal tends to locally flatten the surface a bit due to the larger distances between surface atoms. The shift of the reaction probability curve to lower energies can be understood as well. Nattino *et al.*[20] found a decrease of the barrier height as the crystal was expanded. For $T_s = 925\,\mathrm{K}$, a decrease of the lowest barrier to dissociation, the bridge to hollow bar-

rier, of about 3.5 kJ/mol was found. The decrease found here is somewhat larger (up to approximately 5 kJ/mol) and J-dependent, as will become clear later.

In figure 3.6 the reaction probability for a number of initial rovibrational states is shown, with both thermal displacement and thermal expansion taken into account. The agreement with experiment here is in general significantly better than in figure 3.3, where only thermal displacement was taken into account. The effects seem to be in particular large for ($\nu = 1, J = 0$) H_2, where most of the broadening caused by the thermal displacement has vanished. In general, however, in particular for higher J the agreement is quite good, and the computed $T_s = 925$ K curves mostly line up with the experiments at low incidence energies.

In figure 3.7 the reaction probability is shown for the same two states as in figure 3.4. The curves for $T_s = 925$ K seem to be somewhat too broad, but not by much. The broadening found here is still bigger than the broadening found in the AIMD calculations by Nattino *et al.*[20] The point where the $T_s = 925$ K curve intersects the ideal lattice curve is however in reasonable agreement with the AIMD calculations. It is however noted that the agreement with experiment seems to be better than the AIMD calculations, especially for low energies for ($\nu = 1, J = 6$) D_2.

3.3.2.3 Comparison to desorption experiments

To make a full comparison with the desorption experiments by Rettner *et al.*,[32] Michelsen *et al.*,[28,29] and Murphy and Hodgson,[30] first the similarities and differences in the experimental results are discussed. All of the experimental sticking curves were originally fitted to the form of equation (3.15). Nattino *et al.*[21] re-analysed the experimental sticking curves of Michelsen *et al.*[29] for D_2 on Cu(111) by fitting to a different functional form, which resulted in a higher saturation value for $\nu = 0$. The analysis below is based on the original sticking curves which were fitted to equation (3.15). Michelsen *et al.*[28,29] and Rettner *et al.*[32] measured the desorption probability for a large number of final states, allowing them to determine the A parameter by fitting to adsorption experiments (which yield, in contrast to desorption experiments, absolute reaction probabilities). Murphy and Hodgson[30] only measured the de-

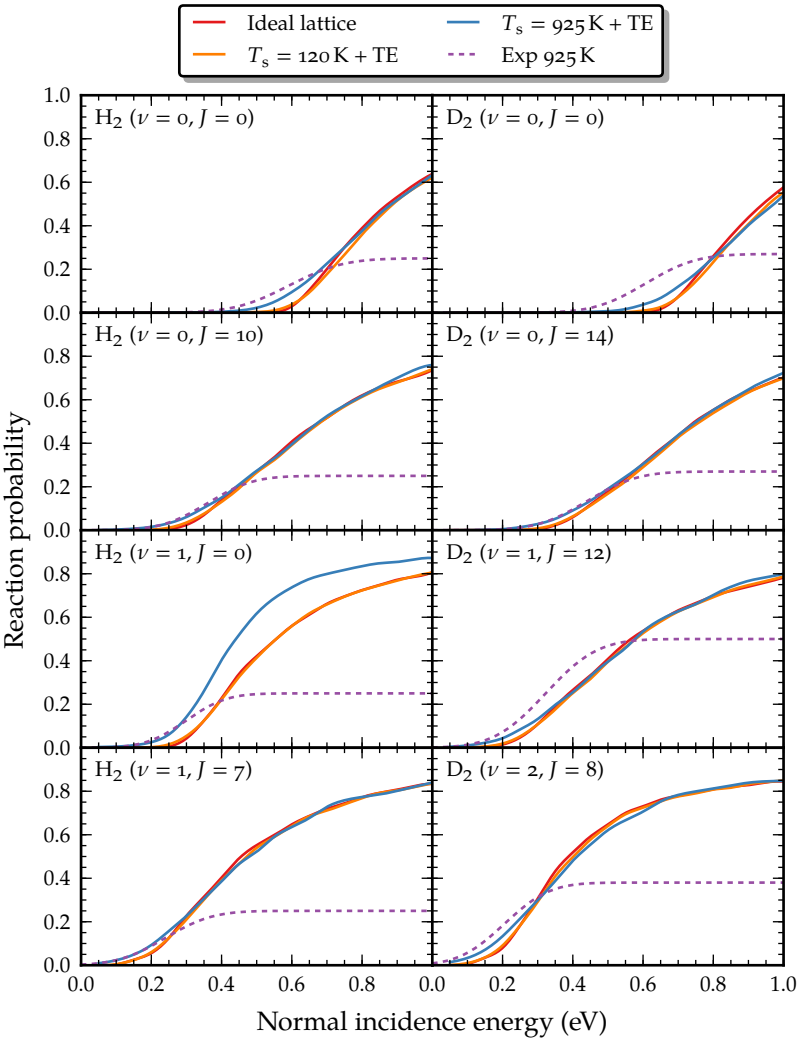

Figure 3.6 Broadening of the sticking curves as the surface temperature is increased, for a selection of initial rovibrational states, taking into account the effects of thermal displacement and thermal expansion (TE) effects. Also plotted are the experimental sticking curves obtained by Michelsen *et al.*[28,29] and Rettner *et al.*[32]

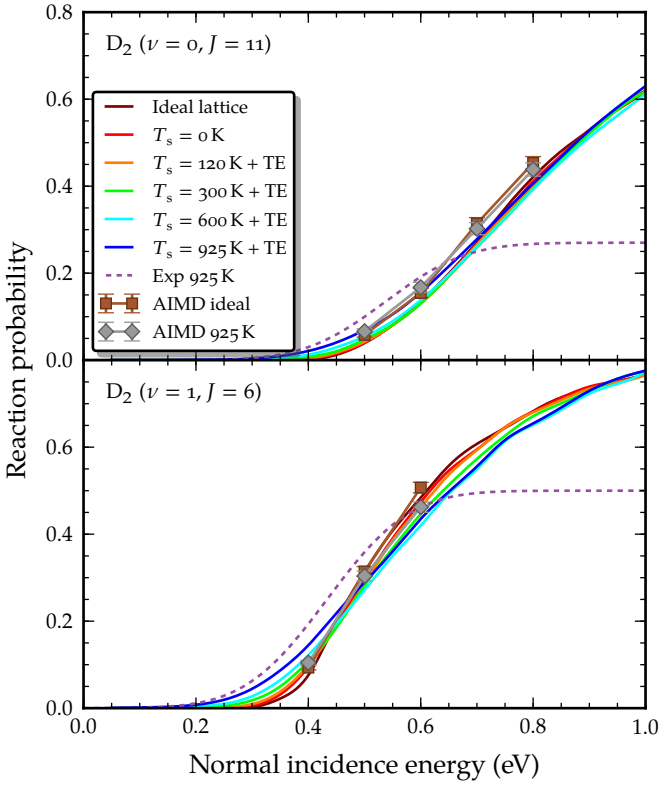

Figure 3.7 Broadening of the sticking curve for D_2 initially in the ($\nu = 0$, $J = 11$) and ($\nu = 1$, $J = 6$) states, for all considered surface temperatures, taking into account the effects of thermal displacement and thermal expansion (TE). The experimental sticking curve[29] is also plotted, as well as the AIMD results by Nattino *et al.*[20]

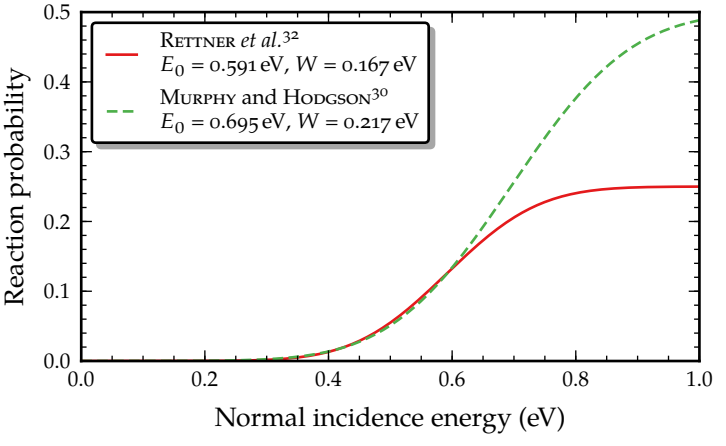

Figure 3.8 Comparison of the sticking curves for ($\nu = 0, J = 5$) H_2 by Murphy and Hodgson[30] and Rettner *et al.*[32] The saturation value for the experiment by Murphy and Hodgson[30] is unknown, and if this would be approximately 0.5 the two experiments are in agreement with each other.

sorption probability for a few final states, which means only E_0 and W were determined. Murphy and Hodgson[30] found significantly larger E_0 and W parameters than Michelsen *et al.*[28,29] and Rettner *et al.*,[32] but no explanation was offered for this.

A possible explanation could be that the sticking curves by Murphy and Hodgson[30] have a higher saturation value. In figure 3.8 the sticking curves of Murphy and Hodgson[30] and Rettner *et al.*[32] for ($\nu = 0$, $J = 5$) H_2 are compared, taking for A the value which gives best agreement between the two different experiments. At low energies, the two curves are essentially the same up to experimental precision. This can be argued to be the most important region for the comparison due to the population of low energies being highest. This shows therefore that the two experiments *could* be in agreement with each other, but it cannot be rigorously proven.

In figure 3.9 the reaction probability for ($\nu = 0, J = 5$) H_2 computed with the model at $T_s = 925\,\mathrm{K}$ is plotted both on a linear scale and on a logarithmic scale. Fits are also shown if A is kept fixed during the fitting procedure for two A parameters. It is shown that the reaction

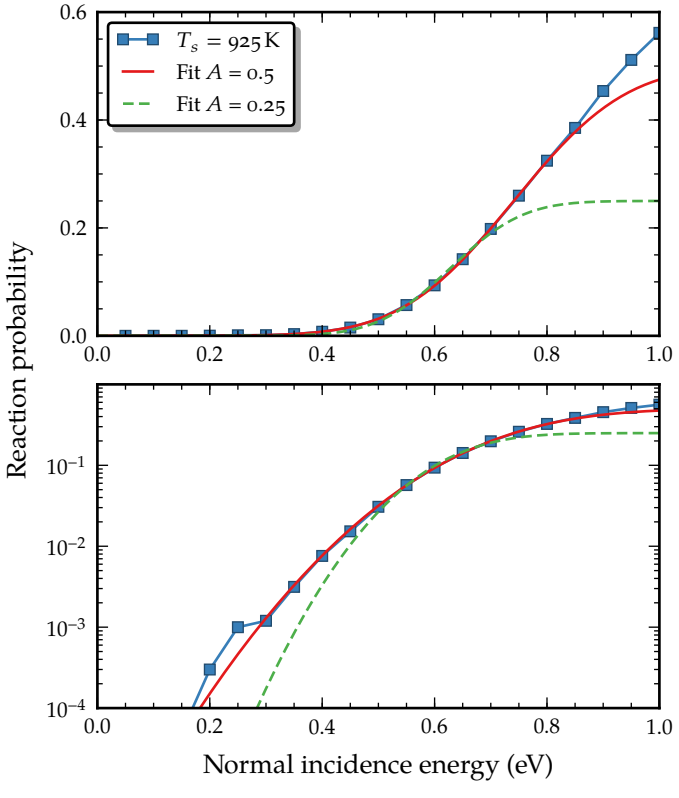

Figure 3.9 Fits for the computed sticking curve at $T_s = 925\,K$ for ($v = 0$, $J = 5$) H_2 with $A = 0.25$, the experimental value reported by Rettner *et al.*,[32] and $A = 0.5$, which yields a much better description of the computed sticking curve.

probability can be well described by the form of equation (3.15), however, if the A parameter determined by Michelsen *et al.* is used the low energy regime is not described well, but also the high energy regime is not described well. Although a low energy "tail" is known,[30] the calculations show a larger difference between the fit to equation (3.15) and the computed values. In fact, it is found that increasing A in the fitting procedure provides a significantly better description of the sticking curve. The similarity between the A value used here (0.5) and the A value used to reconcile the fits of Michelsen *et al.* and those of Murphy and Hodgson[30] is pointed out (see figure 3.8).

As shown in figure 3.9, the calculated sticking curve can be well represented by equation (3.15). If E_0 is fixed to a particular value, W determines the shape of the sticking curve and E_0 its position on the energy axis. Therefore, if W and E_0 are obtained from accurate fits with an A equal to the experimentally found saturation value, a reasonable comparison can be made with experiment. As noted earlier, a higher A value generally provides a better description of the curve at low energies, however in that case no comparison can be made with the experimental data, as E_0 and W will in this case be too high. In the fits below A will be assumed to be equal to the values reported by Michelsen *et al.* and Rettner *et al.* In the fits, data points with a reaction probability smaller than 1% are not taken into account for accuracy reasons; data points with a reaction probability larger than $0.6 \cdot A$ are also not taken into account as they decrease the quality of the description at lower energies, where the population is highest in desorption experiments. Díaz *et al.*[1,2] found that, for the ideal lattice, the fits start to deviate from the computed reaction probabilities above a reaction probability of about $0.75 \cdot A$.

In figure 3.10 the fit parameters are shown for D_2 with $A = 0.27$ ($v = 0$), $A = 0.5$ ($v = 1$) and $A = 0.38$ ($v = 2$). The behaviour of the model with thermal expansion and expansion or contraction of the first interlayer distance is somewhat suspicious for low J ($J < 4$). Although the dynamical barrier height E_0 at $J = 0$ is considerably more decreased than E_0 at high J when the surface temperature is increased, this seems to not be the case for $J = 1$, where it is unchanged or even increased. The curves for E_0 versus rotational state are therefore not as smooth as one might expect. This could be due to the use of a PES for the 6D system with p6mm symmetry, while the symmetry in reality is p3m1. p3m1 symmetry has to be assumed for the surface atom position vectors in the model. Because this could change the anisotropy of the PES, thermal expansion could introduce an error in the PES for the J dependency. Additionally, the pair potential as used in the present model might be too restrictive for correcting for thermal expansion. The effects of thermal expansion are again underlined here: the dynamical barrier height is decreased (system becomes more reactive), while at the same time the width decreases. Overall, the W parameter determining

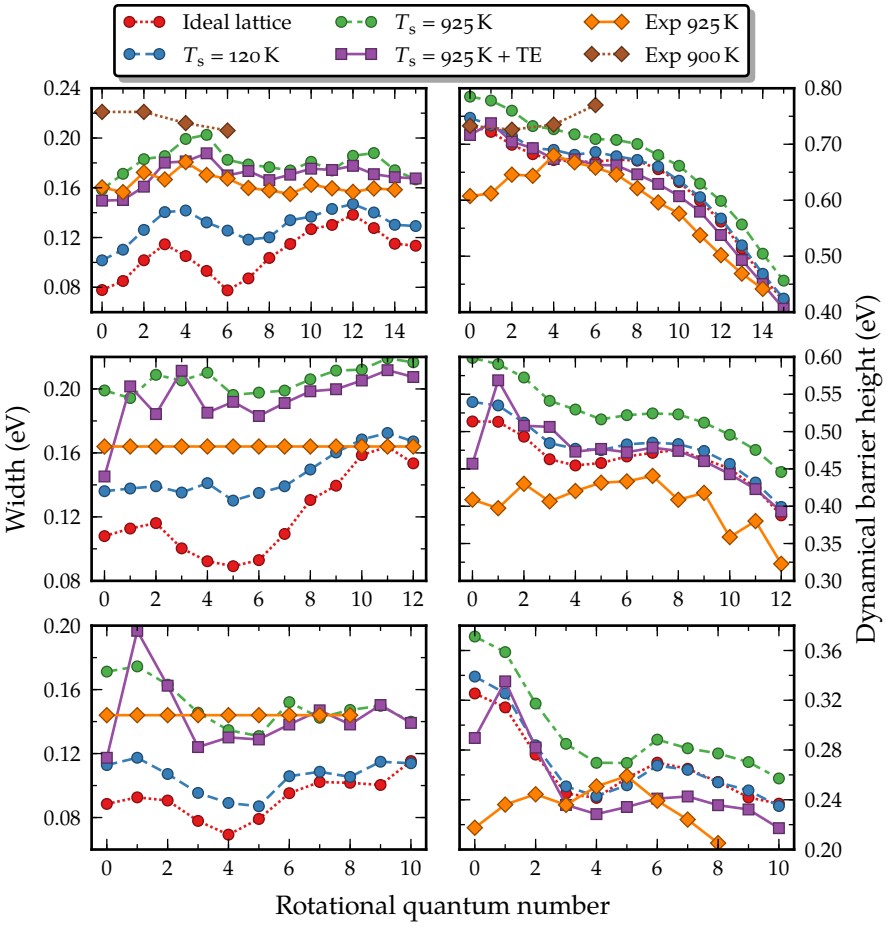

Figure 3.10 Fitted parameters to equation (3.15) for all considered initial states of D_2. Results including thermal expansion are listed as TE. Top panels: ($v = 0$). Middle panels: ($v = 1$). Bottom panels: ($v = 2$). Experimental data with $T_s = 925\,K$ by Michelsen *et al.*[28,29] Experimental data with $T_s = 900\,K$ by Murphy and Hodgson.[30]

the shape of the reaction probability curve is in good agreement with the experiments by Michelsen *et al.*,[28,29] except for ($\nu = 1$), where it is somewhat too large. It is however noted that significant errors in the ratios of A from the experiments ($A(\nu = 0) : A(\nu = 1) : A(\nu = 2) = (0.54 \pm 0.16) : 1.00 : (0.77 \pm 0.18)$)[29] manifest itself here in terms of the W parameters as A was assumed to be fixed to the experimentally reported value. For example, if $A(\nu = 1)$ is assumed to be slightly smaller (0.4 instead of 0.5) the agreement for the width is as good as for other states and the decrease of A is (almost) within the reported errors of the ratios. Overall, the agreement for the E_0 parameter determining the position of the reaction probability curve on the energy axis is improved if also thermal expansion and expansion or contraction of the first interlayer distance is taken into account, but not if only thermal displacement is taken into account. Although the high J behaviour seems good, the low J behaviour is suspicious. Again here for ($\nu = 1$) D_2 the agreement is not so good, but if A is adjusted to 0.4 the agreement is again very good.

In figure 3.11 the fit parameters are shown for H_2 with $A = 0.25$. The agreement with the experiments by Rettner *et al.*[32] is less good than for D_2. It is possible that this could be caused by the use of quasi-classical rather than quantum dynamics. Because H_2 has a lower mass than D_2, quantum effects are more important for H_2 due to this mass difference. Previously with the BOSS model[1,2] significant differences were found between results obtained with quasi-classical and quantum dynamics for H_2 dissociating on Cu(111). Similar effects as found in the results for D_2 above are also found for H_2. Overall the agreement with experiment is good, but for ($\nu = 1$) H_2 the agreement is less good than for ($\nu = 0$) H_2.

Compared to results reported in the literature[1,8,27,30,32,45] for SM[46,47] and (M)SO[42–48] models, significantly better width values are obtained. If the SM model were to be applied on top of the model applied here, only a small amount of extra broadening would be expected, due to the unfavourable H_2/Cu mass ratio. Darling and Holloway[8] already reported in 1994 that the static corrugation which is introduced by thermal displacement of surface atoms could be very important.

Clearly the presented results are sensitive to the accuracy of the experimentally obtained A value. A better comparison would be to

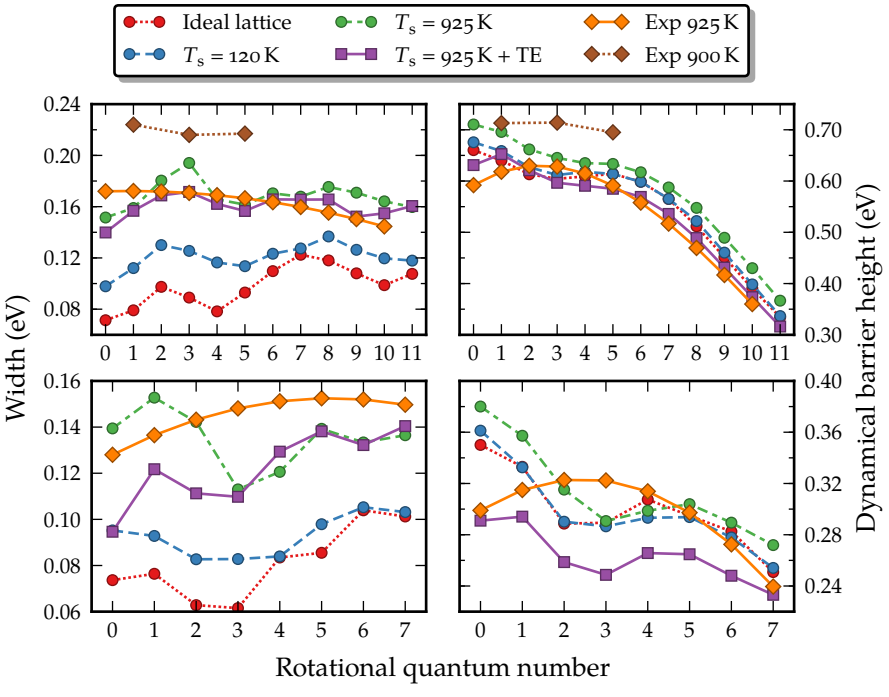

Figure 3.11 Fitted parameters to equation (3.15) for all considered initial states of H_2. Results including thermal expansion are listed as TE. Top panels: ($v = 0$). Bottom panels: ($v = 1$). Experimental data with $T_s = 925$ K by Rettner *et al.*[32] Experimental data with $T_s = 900$ K by Murphy and Hodgson.[30]

compare the theoretical results directly to the raw experimental time-of-flight (TOF) data from which the A, W and E_0 parameters were indirectly extracted. Such a direct comparison has for example been done in 2014 for AIMD calculations on H_2/Cu(111).[21]

3.3.3 Rotational quadrupole alignment parameter

The rotational quadrupole alignment parameter for D_2 desorbing from a Cu(111) surface was measured by Gulding *et al.*,[24] Hou *et al.*,[25] and Wetzig *et al.*[34] The rotational quadrupole alignment parameter is a measurement of preference of desorption in a particular m_J state and the definition of this parameter is given by equation (2.33). Equa-

tion (2.34) shows how it can be computed from the initial state-resolved reaction probability.

Hou *et al.*[25] measured the energy-resolved rotational quadrupole alignment parameter for desorption into two states, while Gulding *et al.*[24] and Wetzig *et al.*[34] measured the rotational quadrupole alignment parameter for desorption into a larger number of states, but these measurements were not energy-resolved. In this study only the energy-resolved rotational quadrupole alignment parameter is considered due to sampling-related inaccuracies of (quasi-)classical methods at low energies.

In figure 3.12 the rotational quadrupole alignment parameter is plotted for a variety of models, comparing the ideal lattice results with the results of the static corrugation model, the experimental data and recent AIMD calculations. The effect of thermal displacement is also a broadening of the rotational quadrupole alignment parameter curve; at low energies the rotational quadrupole alignment parameter is considerably decreased, while at high energies the rotational quadrupole alignment parameter is slightly increased. Including thermal expansion effects in the calculations tends to lead to a further decrease of the rotational quadrupole alignment parameter. Comparing the static corrugation model results with the experimental results, the agreement at low energies is considerably improved, although the observed effect is slightly too large for ($\nu = 1, J = 6$) D_2. At high energies however, the agreement is not improved. It is not clear why this is the case. It is however noted that the experimentalists have calculated the rotational quadrupole alignment parameter from fits to TOF spectra, and these fits may be, like the fits for the desorption probability considered in section 3.3.2, relatively insensitive to the high energy regime, although this does not seem to be reflected in the size of the experimental error bars.

The dependence of the rotational quadrupole alignment parameter on the surface temperature can be explained. It is likely that the arguments (see section 3.3.2) for the broadening and shifting of the J-resolved reaction probability curve also hold for the m_J-resolved reaction probability curves. The calculations done here are in agreement with this. At low energies, the overall reaction probability is increased with increasing surface temperature. This leads to a larger denomin-

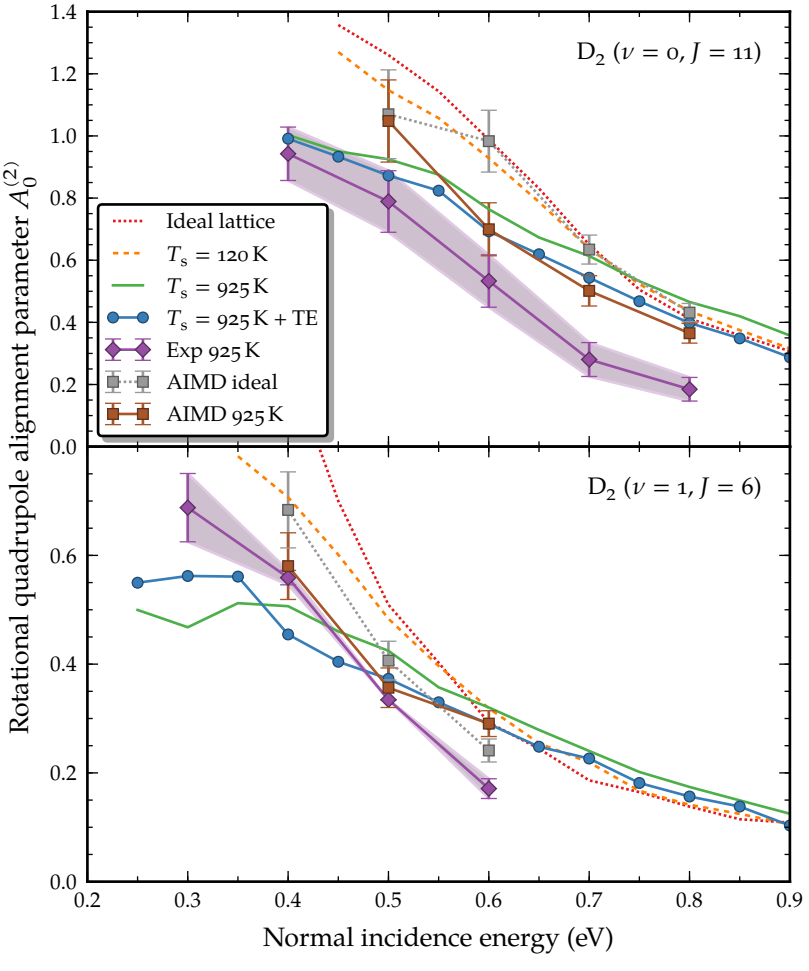

Figure 3.12 Comparison of the rotational quadrupole alignment parameter computed with different models. Plotted are the rotational quadrupole alignment parameter for an ideal crystal, for a crystal with $T_s = 120\,K$, $T_s = 925\,K$, $T_s = 925\,K$ with thermal expansion effects (TE), the experimental data by Hou *et al.*[25] and the AIMD results by Nattino *et al.*,[20] for a rigid ideal surface and moving surface at $T_s = 925\,K$.

ator in equation (2.34). The numerator will decrease because tilted molecules will react more due to the locally tilted surface. This results in a lower alignment parameter. At high energies, the overall reaction probability is only slightly decreased, resulting in a slightly lower denominator. In the limit of saturation (reaction probability equal to unity), the first molecules to react less are the unfavourably tilted ones, resulting in a slightly higher numerator. Overall this leads to a slight increase of the alignment parameter.

3.3.4 Molecular beams

To make a comparison with molecular beam experiments possible, two things have to be taken into account. First, the state-resolved reaction probabilities should be averaged over all states with significant population in the beam. Second, the experimental spread in incidence energies has to be taken into account. The way in which this has been done has been described in section 2.5.3 of this thesis.

Experiments were performed for D_2 by Michelsen *et al.*[29] and for H_2 by Rettner *et al.*[32] The parameters for the velocity distribution, equation (2.39), for these experiments were obtained by Díaz *et al.*[1,2] In the calculations all rovibrational states listed in table 3.2 are included.

In figure 3.13 the molecular beam simulations are shown for the ideal lattice and for $T_s = 120\,\mathrm{K}$. For $T_s = 120\,\mathrm{K}$ the results are not changed much if thermal expansion effects are taken into account: only a slight increase in reaction is found due to the small shift of the reaction probability curve to lower energies. For low average collision energies, reaction is generally found to be slightly increased for $T_s = 120\,\mathrm{K}$ with respect to the ideal lattice, while for higher average collision energies reaction is generally found to be slightly decreased. Comparing the results found here with the AIMD results for this trend is difficult, as no calculations were performed for the ideal lattice and the surface temperature effects are very small. It is noted that the differences found for the initial state-resolved reaction probability of D_2 in the $(v = 0, J = 11)$ state between the SRP potential[1,2] as used here and the AIMD calculations[20] (figure 3.4), might have a consequence for the molecular beam results. The AIMD results for this state were found to be more reactive

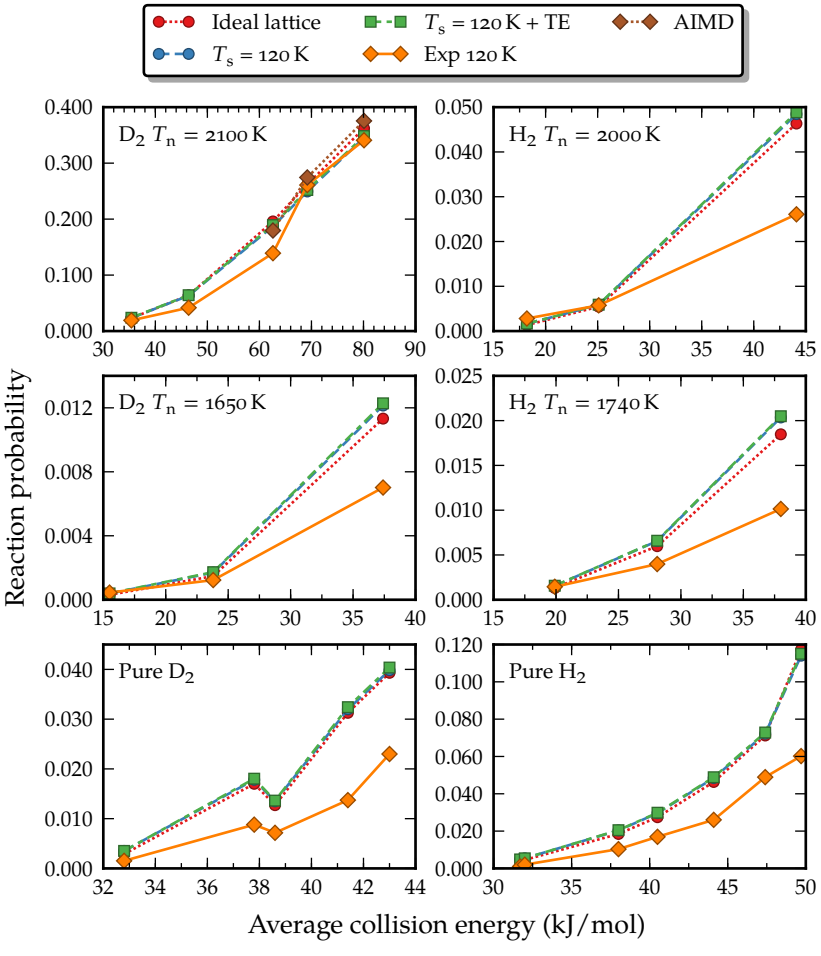

Figure 3.13 Effect of surface temperature on molecular beams, with (TE) and without thermal expansion effects, for a variety of H_2 and D_2 beams. Experiments for D_2 by Michelsen *et al.*[29] and for H_2 by Rettner *et al.*[32] Parameters for the velocity distribution of the molecular beams were extracted by Díaz *et al.*[1,2] *Ab initio* molecular dynamics results by Nattino *et al.*[20]

than the results with the SRP potential used here. If this effect is general for D_2 in the ($\nu = 0$) state, a significant shift should be observed in the molecular beam results. Combined with the significant error in the AIMD results due to a limited number of trajectories being sampled in AIMD, the conclusion here is that the AIMD results are consistent with the results for the static corrugation model.

3.4 Conclusions

A model has been constructed to take into account surface temperature effects for H_2 or D_2 dissociating on a Cu(111) surface. The model is general and does not require a special form for the PES. It is based on the assumption that in different scattering events the hydrogen molecule experiences different non-ideal but (almost) static surfaces. This approximation is reasoned to work well, based on the physics of the event taking place and is corroborated by previous calculations on CH_4 dissociation on metal surfaces. The model introduces a correction term for displacement of surface atoms based on the coupling potential.

The quality of the model has been assessed based on a comparison with a recent DFT study and the comparison of three computed observables with experiments and recent AIMD calculations. The observables that were considered are the initial state-resolved reaction probability, the rotational quadrupole alignment parameter and the reaction probability averaged over the distribution in molecular beams. Overall, the agreement with experiments and the AIMD calculations is found to be good. Apparently bigger overall effects are found here than were found in AIMD calculations, however. The agreement with experiment seems however to be better in some cases for the calculations performed in this work. It is not fully clear why this happens. A possible explanation could be differences in the sampling of surface configurations. For the AIMD calculations a limited number of surface configurations are sampled whereas here surface atoms are displaced individually per trajectory according to a model based on DW factors. The model also differs from AIMD in a different way: whereas in AIMD a 2×2 unit cell is used, here no periodic boundary conditions are applied to the surface atoms. The 1D correction function is relatively long range ($7.5\,a_0$),

which might indicate a larger unit cell might be needed.

For the comparison with the DFT study it is concluded that the chosen form for the 1D correction potential can reproduce well the behaviour of the coupling potential at high-symmetry barrier positions in an ideal surface for perpendicular displacements.

For the initial state-resolved reaction probability, it is found that both thermal displacement and thermal expansion are of importance. Thermal displacement causes the broadening that has been experimentally observed as the surface temperature increases, whereas thermal expansion primarily makes the system more reactive by shifting the reaction probability curves. The discrepancy between two sets of experimental data has been attributed to the fact that experimentalists are not able to measure absolute desorption probabilities. Therefore the experimentalists had to obtain one parameter from a fit to adsorption experiments, which was not done for one of the experiments. The agreement with the AIMD calculations is reasonable, but somewhat broader reaction probability curves are found here. The width of these curves is however generally found to be in agreement with the experiments.

For the rotational quadrupole alignment parameter, it is found that, analogous to the reaction probability, thermal displacement tends to broaden the rotational quadrupole alignment parameter curve, whereas thermal expansion tends to shift the curve. At low energies, the rotational quadrupole alignment parameter is decreased with increasing surface temperature, whereas at high energies, the rotational quadrupole alignment parameter is slightly increased with increasing surface temperature. The agreement with experiment is good at low energies, but less good at high energies. In recent AIMD calculations a decrease with increasing surface temperature was also found at low energies, and one state considered also showed an increase at high energies. A larger broadening of the rotational quadrupole alignment parameter curve is found in the calculations performed here, which provides a better agreement with experiments at low energies.

For the comparison to molecular beam sticking experiments, it is found that the approximation of an ideal surface being representative of a low temperature surface, as previously used, is good. This was also found in recent AIMD calculations. Only very weak surface temperat-

ure effects are found in the molecular beam simulations, in which the surface temperature is 120 K.

The model constructed here is therefore able to reproduce most of the surface temperature effects observed experimentally, without energy exchange between the molecule and the surface being possible. It has been previously suspected, based on model calculations by Darling and Holloway,[8] that the effect of static corrugation could be important, and the calculations performed confirm that idea.

References

[1] C. Díaz, R. A. Olsen, D. J. Auerbach, and G. J. Kroes. Six-dimensional dynamics study of reactive and non reactive scattering of H_2 from Cu(111) using a chemically accurate potential energy surface. *Physical Chemistry Chemical Physics* **12**(24), pp. 6499–6519, 2010.

[2] C. Díaz, E. Pijper, R. A. Olsen, H. F. Busnengo, D. J. Auerbach, and G. J. Kroes. Chemically accurate simulation of a prototypical surface reaction: H_2 dissociation on Cu(111). *Science* **326**(5954), pp. 832–834, 2009.

[3] J. Dai and J. C. Light. The steric effect in a full dimensional quantum dynamics simulation for the dissociative adsorption of H_2 on Cu(111). *Journal of Chemical Physics* **108**(18), pp. 7816–7820, 1998.

[4] J. Dai and J. C. Light. Six dimensional quantum dynamics study for dissociative adsorption of H_2 on Cu(111) surface. *Journal of Chemical Physics* **107**(5), pp. 1676–1679, 1997.

[5] J. Dai, J. Sheng, and J. Z. H. Zhang. Symmetry and rotational orientation effects in dissociative adsorption of diatomic molecules on metals: H_2 and HD on Cu(111). *Journal of Chemical Physics* **101**(2), pp. 1555–1563, 1994.

[6] J. Dai and J. Z. H. Zhang. Quantum adsorption dynamics of a diatomic molecule on surface: Four-dimensional fixed-site model for H_2 on Cu(111). *Journal of Chemical Physics* **102**(15), pp. 6280–6289, 1995.

[7] J. Dai and J. Z. H. Zhang. Steric effect in dissociative chemisorption of hydrogen on Cu. *Surface Science* **319**(1–2), pp. 193–198, 1994.

[8] G. R. Darling and S. Holloway. Surface temperature effects in the dissociative adsorption of D_2/Cu(111) revisited. *Surface Science* **321**(3), pp. L189–L194, 1994.

[9] G. R. Darling and S. Holloway. Rotational motion and the dissociation of H_2 on Cu(111). *Journal of Chemical Physics* **101**(4), pp. 3268–3281, 1994.

[10] G. R. Darling and S. Holloway. Dissociation thresholds and the vibrational excitation process in the scattering of H_2. *Surface Science* **307–309**(A), pp. 153–158, 1994.

[11] G. R. Darling and S. Holloway. Translation-to-vibrational excitation in the dissociative adsorption of D_2. *Journal of Chemical Physics* **97**(1), pp. 734–736, 1992.

[12] A. Forni, G. Wiesenekker, E. J. Baerends, and G. F. Tantardini. A dynamical study of the chemisorption of molecular hydrogen on the Cu(111) surface. *Journal of Physics: Condensed Matter* **7**(36), pp. 7195–7207, 1995.

[13] A. Forni, G. Wiesenekker, E. J. Baerends, and G. F. Tantardini. The chemisorption of hydrogen on Cu(111): a dynamical study. *International Journal of Quantum Chemistry* **52**(4), pp. 1067–1080, 1994.

[14] A. Gross, B. Hammer, M. Scheffler, and W. Brenig. High-dimensional quantum dynamics of adsorption and desorption of H_2 at Cu(111). *Physical Review Letters* **73**(23), pp. 3121–3124, 1994.

[15] B. Hammer, M. Scheffler, K. W. Jacobsen, and J. K. Nørskov. Multidimensional potential energy surface for H_2 dissociation over Cu(111). *Physical Review Letters* **73**(10), pp. 1400–1403, 1994.

[16] S. Nave, D. Lemoine, M. F. Somers, S. M. Kingma, and G. J. Kroes. Six-dimensional quantum dynamics of (v = 0, j = 0) D_2 and of (v = 1, j = 0) H_2 scattering from Cu(111). *Journal of Chemical Physics* **122**(21), 214709, 2005.

[17] U. Nielsen, D. Halstead, S. Holloway, and J. K. Nørskov. The dissociative adsorption of hydrogen: two-, three-, and four-dimensional quantum simulations. *Journal of Chemical Physics* **93**(4), pp. 2879–2884, 1990.

[18] J. Sheng and J. Z. H. Zhang. Quantum dynamics studies of adsorption and desorption of hydrogen at a Cu(111) surface. *Journal of Chemical Physics* **99**(2), pp. 1373–1381, 1993.

[19] M. F. Somers, S. M. Kingma, E. Pijper, G. J. Kroes, and D. Lemoine. Six-dimensional quantum dynamics of scattering of (v = 0, j=0) H_2 and D_2 from Cu(111): test of two LEPS potential energy surfaces. *Chemical Physics Letters* **360**(3–4), pp. 390–399, 2002.

[20] F. Nattino, C. Díaz, B. Jackson, and G. J. Kroes. Effect of surface motion on the rotational quadrupole alignment parameter of D_2 reacting on Cu(111). *Physical Review Letters* **108**(23), 236104, 2012.

[21] F. Nattino, A. Genova, M. Guijt, A. S. Muzas, C. Díaz, D. J. Auerbach, and G. J. Kroes. Dissociation and recombination of D_2 on Cu(111): *ab initio* molecular dynamics calculations and improved analysis of desorption experiments. *Journal of Chemical Physics* **141**(12), 124705, 2014.

[22] G. Anger, A. Winkler, and K. D. Rendulic. Adsorption and desorption kinetics in the systems H_2/Cu(111), H_2/Cu(110) and H_2/Cu(100). *Surface Science* **220**(1), pp. 1–17, 1989.

[23] H. F. Berger, M. Leisch, A. Winkler, and K. D. Rendulic. A search for vibrational contributions to the activated adsorption of H_2 on copper. *Chemical Physics Letters* **175**(5), pp. 425–428, 1990.

[24] S. J. Gulding, A. M. Wodtke, H. Hou, C. T. Rettner, H. A. Michelsen, and D. J. Auerbach. Alignment of D_2(v, J) desorbed from Cu(111): low sensitivity of activated dissociative chemisorption to approach geometry. *Journal of Chemical Physics* **105**(21), pp. 9702–9705, 1996.

[25] H. Hou, S. J. Gulding, C. T. Rettner, A. M. Wodtke, and D. J. Auerbach. The stereodynamics of a gas-surface reaction. *Science* **277**(5322), pp. 80–82, 1997.

[26] H. A. Michelsen and D. J. Auerbach. A critical examination of data on the dissociative adsorption and associative desorption of hydrogen at copper surfaces. *Journal of Chemical Physics* **94**(11), pp. 7502–7520, 1991.

[27] H. A. Michelsen, C. T. Rettner, and D. J. Auerbach. State-specific dynamics of D_2 desorption from Cu(111): the role of molecular rotational motion in activated adsorption-desorption dynamics. *Physical Review Letters* **69**(18), pp. 2678–2681, 1992.

[28] H. A. Michelsen, C. T. Rettner, and D. J. Auerbach. On the influence of surface temperature on adsorption and desorption in the D_2/Cu(111) system. *Surface Science* **272**(1–3), pp. 65–72, 1992.

[29] H. A. Michelsen, C. T. Rettner, D. J. Auerbach, and R. N. Zare. Effect of rotation on the translational and vibrational energy dependence of the dissociative adsorption of D_2 on Cu(111). *Journal of Chemical Physics* **98**(10), pp. 8294–8307, 1993.

[30] M. J. Murphy and A. Hodgson. Adsorption and desorption dynamics of H_2 and D_2 on Cu(111): the role of surface temperature and evidence for corrugation of the dissociation barrier. *Journal of Chemical Physics* **108**(10), pp. 4199–4211, 1998.

[31] C. T. Rettner, D. J. Auerbach, and H. A. Michelsen. Role of vibrational and translational energy in the activated dissociative adsorption of D_2 on Cu(111). *Physical Review Letters* **68**(8), pp. 1164–1167, 1992.

[32] C. T. Rettner, H. A. Michelsen, and D. J. Auerbach. Quantum-state-specific dynamics of the dissociative adsorption and associative desorption of H_2 at a Cu(111) surface. *Journal of Chemical Physics* **102**(11), pp. 4625–4641, 1995.

[33] C. T. Rettner, H. A. Michelsen, and D. J. Auerbach. Determination of quantum-state-specific gas-surface energy transfer and adsorption probabilities as a function of kinetic energy. *Chemical Physics* **175**(1), pp. 157–169, 1993.

[34] D. Wetzig, M. Rutkowski, R. David, and H. Zacharias. Rotational corrugation in associative desorption of D_2 from Cu(111). *Europhysics Letters* **36**(1), pp. 31–36, 1996.

[35] P. Nieto, E. Pijper, D. Barredo, G. Laurent, R. A. Olsen, E. J. Baerends, G. J. Kroes, and D. Farías. Reactive and nonreactive scattering of H_2 from a metal surface is electronically adiabatic. *Science* **312**(5770), pp. 86–89, 2006.

[36] A. Gross and A. Dianat. Hydrogen dissociation dynamics on precovered Pd surfaces: Langmuir is still right. *Physical Review Letters* **98**(20), 206107, 2007.

[37] F. R. Kroeger and C. A. Swenson. Absolute linear thermal-expansion measurements on copper and aluminum from 5 to 320 K. *Journal of Applied Physics* **48**(3), pp. 853–864, 1977.

[38] I. E. Leksina and S. I. Novikova. Thermal expansion of copper, silver, and gold within a wide range of temperatures. *Soviet Physics - Solid State* **5**(4), pp. 798–801, 1963.

[39] K. H. Chae, H. C. Lu, and T. Gustafsson. Medium-energy ion-scattering study of the temperature dependence of the structure of Cu(111). *Physical Review B* **54**(19), pp. 14082–14086, 1996.

[40] V. F. Sears and S. A. Shelley. Debye-Waller factor for elemental crystals. *Acta Crystallographica* **A47**(4), pp. 441–446, 1991.

[41] E. C. Svensson, B. N. Brockhouse, and J. M. Rowe. Crystal dynamics of copper. *Physical Review* **155**(3), pp. 619–632, 1967.

[42] M. Dohle and P. Saalfrank. Surface oscillator models for dissociative sticking of molecular hydrogen at non-rigid surfaces. *Surface Science* **373**(1), pp. 95–108, 1997.

[43] M. Dohle, P. Saalfrank, and T. Uzer. Dissociative sticking of diatomic molecules on cold, non-rigid surfaces: comparison of quantal and semiclassical surface oscillator model. *Surface Science* **409**(1), pp. 37–45, 1998.

[44] M. Dohle, P. Saalfrank, and T. Uzer. The dissociation of diatomic molecules on vibrating surfaces: a semiclassical generalized Langevin approach. *Journal of Chemical Physics* **108**(10), pp. 4226–4236, 1998.

[45] M. Hand and J. Harris. Recoil effects in surface dissociation. *Journal of Chemical Physics* **92**(12), pp. 7610–7617, 1990.

[46] A. C. Luntz and J. Harris. CH_4 dissociation on metals: a quantum dynamics model. *Surface Science* **258**(1–3), pp. 397–426, 1991.

[47] P. Saalfrank and W. H. Miller. Quantum-mechanical rates for gas-surface processes. *Surface Science* **303**(1–2), pp. 206–230, 1994.

[48] H. F. Busnengo, W. Dong, P. Sautet, and A. Salin. Surface temperature dependence of rotational excitation of H_2 scattered from Pd(111). *Physical Review Letters* **87**(12), 127601, 2001.

[49] S. Nave and B. Jackson. Methane dissociation on Ni(111): the effects of lattice motion and relaxation on reactivity. *Journal of Chemical Physics* **127**(22), 224702, 2007.

[50] S. Nave and B. Jackson. Methane dissociation on Ni(111): the role of lattice reconstruction. *Physical Review Letters* **98**(17), 173003, 2007.

[51] N. Pineau, H. F. Busnengo, J. C. Rayez, and A. Salin. Relaxation of hot atoms following H_2 dissociation on a Pd(111) surface. *Journal of Chemical Physics* **122**(21), 214705, 2005.

[52] M. Bonfanti, M. F. Somers, C. Díaz, H. F. Busnengo, and G. J. Kroes. 7D quantum dynamics of H_2 scattering from Cu(111): the accuracy of the phonon sudden approximation. *Zeitschrift für Physikalische Chemie* **227**(11), pp. 1397–1420, 2013.

[53] M. Bonfanti, C. Díaz, M. F. Somers, and G. J. Kroes. Hydrogen dissociation on Cu(111): the influence of lattice motion. Part I. *Physical Chemistry Chemical Physics* **13**(10), pp. 4552–4561, 2011.

[54] A. K. Tiwari, S. Nave, and B. Jackson. The temperature dependence of methane dissociation on Ni(111) and Pt(111): mixed quantum-classical studies of the lattice response. *Journal of Chemical Physics* **132**(13), 134702, 2010.

[55] A. K. Tiwari, S. Nave, and B. Jackson. Methane dissociation on Ni(111): a new understanding of the lattice effect. *Physical Review Letters* **103**(25), 253201, 2009.

[56] H. F. Busnengo, A. Salin, and W. Dong. Representation of the 6D potential energy surface for a diatomic molecule near a solid surface. *Journal of Chemical Physics* **112**(17), pp. 7641–7651, 2000.

[57] R. Drautz, M. Fähnle, and J. M. Sanchez. General relations between many-body potentials and cluster expansions in multicomponent systems. *Journal of Physics: Condensed Matter* **16**(23), pp. 3843–3852, 2004.

[58] J. Ludwig, D. G. Vlachos, A. C. T. van Duin, and W. A. Goddard. Dynamics of the dissociation of hydrogen on stepped platinum surfaces using the ReaxFF reactive force field. *Journal of Physical Chemistry B* **110**(9), pp. 4274–4282, 2006.

[59] P. Valentini, T. E. Schwartzentruber, and I. Cozmuta. Molecular dynamics simulation of O_2 sticking on Pt(111) using the *ab initio* based ReaxFF reactive force field. *Journal of Chemical Physics* **133**(8), 084703, 2010.

[60] Y. Xiao, W. Dong, and H. F. Busnengo. Reactive force fields for surface chemical reactions: A case study with hydrogen dissociation on Pd surfaces. *Journal of Chemical Physics* **132**(1), 014704, 2010.

[61] X. J. Shen, A. Lozano, W. Dong, H. F. Busnengo, and X. H. Yan. Towards bond selective chemistry from first principles: methane on metal surfaces. *Physical Review Letters* **112**(4), 046101, 2014.

[62] J. P. Perdew, J. A. Chevary, S. H. Vosko, K. A. Jackson, M. R. Pederson, D. J. Singh, and C. Fiolhais. Atoms, molecules, solids, and surfaces: applications of the generalized gradient approximation for exchange and correlation. *Physical Review B* **46**(11), pp. 6671–6687, 1992.

[63] B. Hammer, L. B. Hansen, and J. K. Nørskov. Improved adsorption energetics within density-functional theory using revised Perdew-Burke-Ernzerhof functionals. *Physical Review B* **59**(11), pp. 7413–7421, 1999.

[64] B. Verberck. Symmetry-adapted Fourier series for the wallpaper groups. *Symmetry* **4**(3), pp. 379–426, 2012.

[65] C. C. Marston and G. G. Balint-Kurti. The Fourier grid Hamiltonian method for bound state eigenvalues and eigenfunctions. *Journal of Chemical Physics* **91**(6), pp. 3571–3576, 1989.

[66] J. Stoer and R. Bulirsch. *Introduction to numerical analysis*. New York: Springer, 1980.

[67] M. Bonfanti. Personal communication. 2011.

CHAPTER

3